Int. J. Heat Mass Transfer. Vol. 18, pp. 655–669. Pergamon Press 1975. Printed in Great Britain

BUBBLE GROWTH RATES IN NUCLEATE BOILING OF WATER AT SUBATMOSPHERIC PRESSURES

S. J. D. VAN STRALEN, R. COLE,* W. M. SLUYTER and M. S. SOHAL†
Transportphysics Section, Eindhoven University of Technology, Eindhoven, Netherlands

(*Received* 8 *April* 1974)

Abstract—The growth rate of vapour bubbles has been investigated experimentally up to departure in water boiling at pressures varying from 26·7 to 2·0 kPa (the corresponding Jakob number increasing from 108 to 2689).

Comparison of the data with existing theory shows the substantial influence of liquid inertia during initial growth, in agreement with previous results of Stewart and Cole [1] on water boiling at 4·9 kPa, the Jakob number varying from 955 to 1112. As an extreme case, at a pressure of 2·0 kPa, large "Rayleigh" bubbles are observed during the entire adherence time. During advanced growth, bubble behaviour is gradually governed by heat diffusion, especially at relatively high (subatmospheric) pressures.

Experimental bubble growth in the investigated pressure range is in quantitative agreement with the van Stralen, Sohal, Cole and Sluyter theory [10]. This model combines the Rayleigh solution with a diffusion-type solution, which accounts for the contributions to bubble growth due to both the relaxation microlayer (around the bubble dome) and the evaporation microlayer (beneath the bubble).

Finally, a curious bubble cycle is observed at the lowest investigated pressures, which is attributed to the combined action of a high-velocity liquid jet (originating in the wake following a large primary bubble) and a succeeding secondary vapour column (generated at the adjacent dry spot at the heating wall beneath the primary bubble).

NOMENCLATURE

a, liquid thermal diffusivity [m^2/s];
a_w, thermal diffusity of copper [m^2/s];
b, b^*, dimensionless bubble growth parameter during adherence;
$d_{w,co}$, thickness of equivalent conduction boundary layer at heating surface [m];
$d_0\{R_c^*(t_c)\}$, maximum initial thickness of evaporation microlayer [m];
e, $= 2{\cdot}718\ldots$, base of natural logarithms;
F_w/F, ratio of thermal "contact coefficients" of copper and water;
H_1, $= 2b^*R(t_1)$, maximum height of spherical bubble segment covered with relaxation microlayer [m];
Ja, Jakob number;
l, latent heat of vapourization [J/kg];
p, ambient pressure [$Pa = kg/ms^2$];
q_w, heat flux density at heating surface [W/m^2];
R, equivalent spherical bubble radius [m];
$R(t_1)$, equivalent bubble departure radius [m];
R_1, equivalent bubble radius according to (modified) Rayleigh solution [m];
R_2, equivalent bubble radius according to total diffusion (combined evaporation and relaxation microlayer) solution [m];
R_c^*, radius of contact area between bubble and heating surface [m];
R_d^*, radius of dry area beneath bubble [m];
t, time during bubble adherence or during delay [m];
t_1, bubble departure time [s];
t_2, waiting time between succeeding bubbles [m];
t_c, instant at which R_c^* shows a maximum [s];
t_e, instant at which $R_1 = R_2$ [s];
T, absolute boiling temperature [K].

Greek symbols

θ_0, superheating of heating surface [K];
$\Delta\theta_0$, superheating of bulk liquid [K];
ρ_2, saturated vapour density [kg/m^3].

1. PREVIOUS INVESTIGATIONS

1.1 *Experiments*

IN AN experimental study, Stewart and Cole [1] investigated the initial growth rate (during 20 ms) of hemispherical bubbles in water boiling at a constant subatmospheric pressure of 4·9 kPa and a nearly constant Jakob number of 1030 ± 80. The bubbles were generated on the horizontal top face of a copper rod. The influential parameters were kept nearly constant at the following values: $q_w = (16 \pm 1) \times 10^4$ W/m^2, $\theta_0 = (19{\cdot}9 \pm 1{\cdot}6)$ K and $\Delta\theta_0 = (1{\cdot}0 \pm 0{\cdot}1)$ K. Only the waiting time between bubbles varied substantially from 1·7 ms to 1640 ms.

Stewart and Cole [1] compared their results with predictions of existing theoretical models. As anticipated from the earlier results of Cole and Shulman [2], cf. also [3], the data showed substantially lower initial bubble growth as compared to the predictions of the diffusion controlled models, regardless of whether

*Department of Chemical Engineering, Clarkson College of Technology, Potsdam, New York 13676, U.S.A.
†Present address: Department of Thermodynamics and Fluid Mechanics, University of Strathclyde, Glasgow, Scotland.

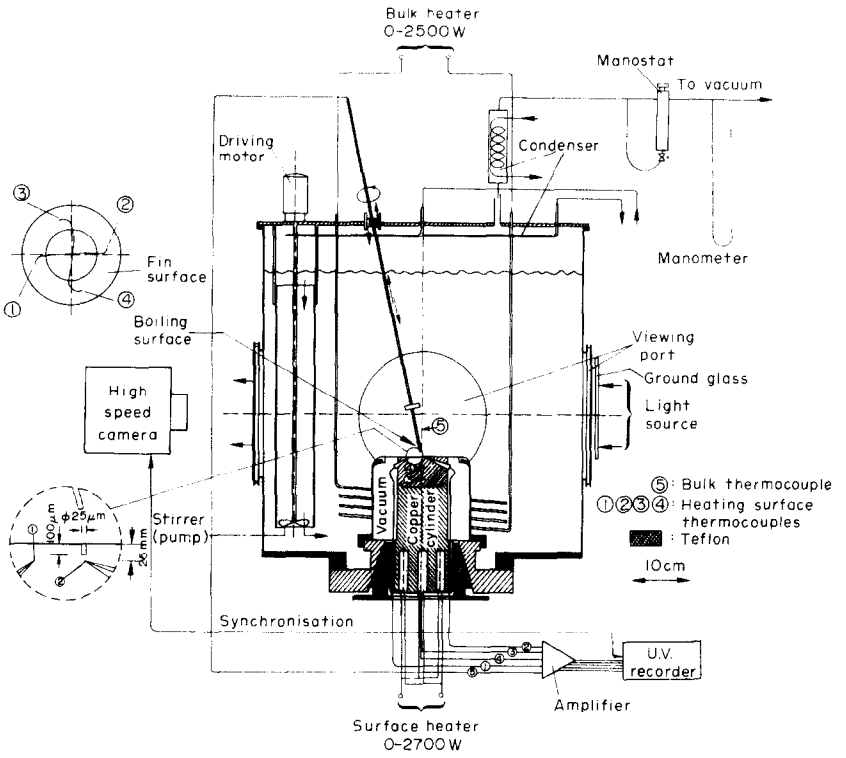

FIG. 1. Diagram of boiling apparatus.

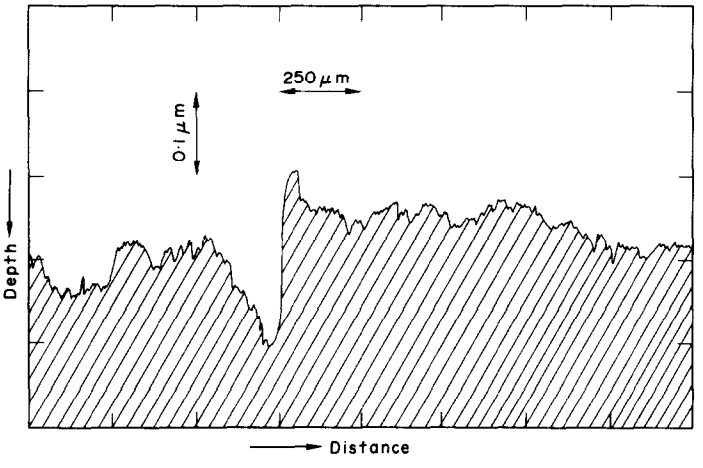

FIG. 2. Roughness of a nickel-plated copper heating surface.

they were of the uniform superheat [4–6], non-uniform superheat, or microlayer type, cf. Section 4.2.

Comparison with two models which included the effect of liquid inertia [7, 8] showed much closer agreement. In both models, the initial hydrodynamic effect of liquid inertia resulting in $R_1 \sim (p\theta_0)^{1/2}t$ (the Rayleigh solution [9]) had been combined with an asymptotic diffusion solution $R_2 \sim (\theta_0/p)t^{1/2}$ due either to evaporation at the bubble dome—Mikic, Rohsenow and Griffith [7] or to evaporation of a hydrodynamically formed thin liquid microlayer beneath the bubble—Cooper and Vijuk [8].

As a consequence, the reduction in initial bubble growth was attributed by Stewart and Cole to liquid inertia, even though reasonable agreement with [8] was observed only for bubbles with a large waiting time and [7] consistently overestimated the experimental growth rates.

1.2 *Theory*

Van Stralen, Sohal, Cole and Sluyter [10] developed a model, which combines the effect of both relaxation microlayer (around the bubble dome) and evaporation microlayer with the Rayleigh solution. The decrease of

the superheating enthalpy of both microlayers during bubble growth is taken into account. Also, in [10], an extensive survey of other theoretical models has been presented.

The dominating role of the relaxation microlayer in the bubble growth process during nucleate boiling at higher pressures has been shown previously by van Stralen [11–13]. Advantages of the relaxation microlayer model in comparison to other theoretical models are: (i) the physical background has been justified directly by experiment [14]; (ii) expressions are derived for both the bubble departure and waiting times, whence the entire bubble history is predictable; (iii) the maximum heat flux in nucleate boiling follows from bubble behaviour and is related to the corresponding convective heat flux; (iv) the model is valid both in superheating and subcooling of pure and of binary boiling systems.

2. PRESENT EXPERIMENTAL INVESTIGATIONS

Vapour bubbles have been studied up to departure in water boiling at subatmospheric pressures ranging from 2 to 27 kPa, the corresponding Jakob number being 2700 to 100. Additional experiments have been carried out with aqueous binary mixtures containing 2-butanone, boiling at a pressure of 5 kPa. The latter results will be published separately [15].

In general, the experiments have been carried out similarly to the procedure given by Stewart and Cole [1]. However, a number of improvements has been made, cf. the next Sections 2.1–2.4.

2.1 *Boiling vessel*

(i) Both the height and the diameter of the cylindrical boiling vessel have been extended to a considerable size of 520 mm (Fig. 1) in order to avoid an instantaneous subcooling of the bulk liquid due to a sudden increase in pressure occurring during rapid initial bubble growth. The pressure was kept constant (within 0·01 kPa in absence of bubbles and within 0·1 kPa during bubble growth) by the combined action of a vacuum pump and a Cartesian manostat.

(ii) The diameters of the copper cylinder and of the thin circular fin at the top face, acting as the heating surface, have been extended to 80 mm and 110 mm, respectively.

The heat source consists of nine adjustable 300 W cartridge beaters embedded in the base of the copper cylinder.

(iii) Unwanted interaction of neighbouring bubbles is avoided by generating single bubbles on a cylindrical artificial nucleation cavity (diameter: 25 μm, depth: 100 μm) created by applying a spark erosion process at the centre of the top face, Fig. 9–(4). The original copper surface showed corrosion at higher calibration temperatures, which resulted in the activation of a number of randomly distributed nucleation sites. This has been removed by smoothing the heating surface (to a roughness within 0·2 μm) with an electrolytically plated nickel layer of 10 μm thickness (Fig. 2) or with a silicon oxide layer of 0·75 μm.

(iv) At the lowest pressure investigated (2 kPa), the required wall superheating for bubble generation on the artificial nucleation site amounts to a practically unattainable value of 100 K (Table 2). In this case, a bubble has been generated by means of a pulsed hot-wire anemometer located in the liquid just above the nucleation site.

(v) The original polymerized urethane thermal insulation around the periphery of the copper cylinder has been replaced by a vacuum insulation, as this resin shows a thermal expansion at higher temperatures in water. This undesirable effect is even much more pronounced in organic liquids, in which the resin is swelling and softening and thus obstructing the filming of initial stage of bubble growth.

2.2 *High speed cinematography*

(i) The boiling vessel has been provided with two mutually perpendicular couples of opposite glass windows to allow simultaneous film exposures with two high speed cameras, a Hitachi (30 m, 16 mm film) rotating-prism camera, operated at 4000 fps (showing a bubble during the entire life-time), and a rotating-mirror Dynafax (1 m, 36 mm film) drum camera, operated at 25 000 fps (showing initial bubble growth more accurately). The ignition of the flashlight (ignition time: 50 μs), which is used in combination with the faster camera, has been triggered to the instant of formation of an equilibrium bubble, by detecting the light interruption of a laser beam (width: 50 μm) with a photocell coupled to an electronic circuit.

(ii) The films were analyzed frame by frame using a Hitachi motion analyzer to obtain quantitative bubble growth data. After an initial mode of hemispherical growth, the bubble shape departs from a hemisphere. Generally, also during advanced growth, the bubble profile remains rotational symmetric. The equivalent radius has been computed then by applying Simpson's rule, cf. [1], i.e. the bubble profile is divided into a limited number of circular discs.

2.3 *Temperature measurements*

(i) Thermocoax chromel–alumel thermocouples (1–5 in Fig. 1) with a stainless steel sheath have been used; the external diameter amounts to 250 μm, the wire diameter to 50 μm. The hot junction is electrically insulated from the sheath. The bulk liquid temperature has been measured with a calibrated mercury-in-glass thermometer, and has also been recorded (at a distance of generally 10 mm above the heating surface) absolutely with respect to the melting point of ice. The accuracy of the thermocouple readings amounts to 0·1 K; this relatively high accuracy is due to the application of a differential circuit, in which a suitable constant voltage is subtracted from the thermocouple emf at the input of a differential amplifier. Care was taken to reduce ripple by using coaxial cables. All other temperatures are taken from recorded mutual differentials. Occasionally, the reliability and the reproducibility of the recordings have been checked by measuring the absolute values, similarly to the bulk

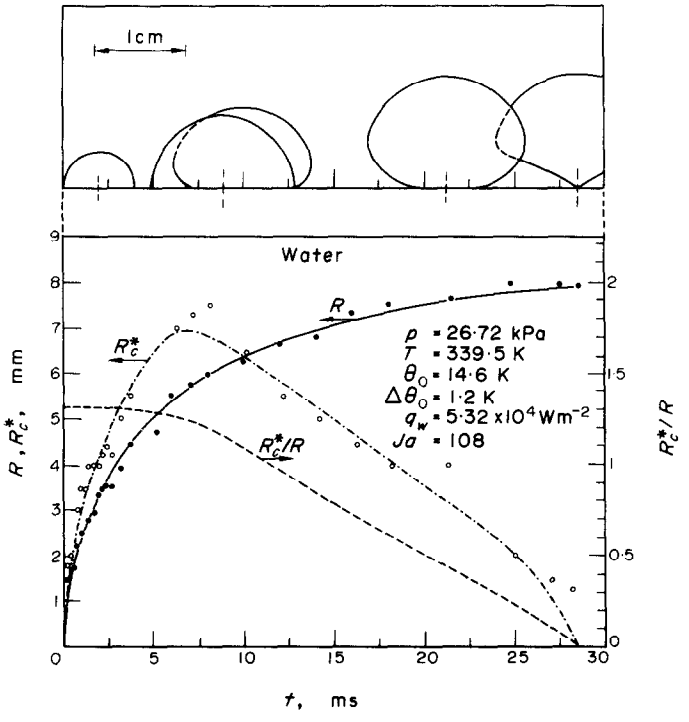

FIG. 3. Water boiling at 26·72 kPa. Equivalent bubble radius, R, contactradius, R_c^*, and ratio, R_c^*/R, in dependence on time. Corresponding bubble profile and limit of mode of hemispherical growth are shown in the upper drawings.

liquid temperature. In addition to the thermocouples located at the axis of the copper cylinder, an extra thermocouple has been placed 20 mm out of the axis with the purpose to estimate the radial heat flux beneath the top surface (Fig. 1). Actually, however, the experimental data showed only negligible radial fluxes.

(ii) Occasionally, at lower pressures, but most pronounced at the lowest pressure investigated (2 kPa), local temperature fluctuations have been observed to occur inside the copper heating material at the locations of the thermocouples beneath the top face of the cylinder. These fluctuations have been synchronized to bubble history.

2.4 *Heat flux at the surface*

The heat flux density at the top face of the cylinder has been determined by extrapolation of simultaneous thermocouple recordings (2–4 in Fig. 1), similarly to the procedure described in [1]. The evaluated temperatures were taken under stationary conditions occurring before sudden generation of a vapour bubble at the artificial nucleation site.

The accuracy of the heat flux measurements amounts to approximately 5 per cent. In general, the heat flux density, evaluated by extrapolation, is 10 per cent lower than the corresponding value, which has been calculated from the applied total electrical power of the cartridge heaters located at the bottom of the copper cylinder (Fig. 1).

3. EXPERIMENTAL RESULTS

3.1 *Bubble growth curves*

Figures 3–8 show the experimental bubble growth curves $R(t)$ up to departure in water boiling at subatmospheric pressures of 27–2 kPa. Detailed information on the values of the influential parameters is given in legends at the figures. The simultaneous bubble profile in dependence on time is drawn at the top of the figures. The limitation of the initial mode of hemispherical growth is denoted by the last picture showing this shape. In general, the experimental results show, that hemispherical growth [Fig. 9–(1, 2, 3)] occurs only during an initial period of 9 ms.

Initial growth is shown in Fig. 10. For $t > 13$ ms, the diffusion solution is dominating apparently at pressures in the range from 4 kPa to 27 kPa, as in the uniform superheat case $R_2 \sim (\theta_0/p)t^{1/2}$; whereas the Rayleigh solution, initially dominating, is giving $R_1 \sim (p\theta_0)^{1/2}t$, cf. equations (9) and (39) of [10]. The different dependence of both solutions on time and pressure—in combination with various experimental values of θ_0—results in complicated growth curves during the mode of early growth.

The instant, t_e, at which $R_1(t_e) = R_2(t_e)$ follows by equating equations (62) and (63) of [10]; t_e is shown in Fig. 12 as a function of pressure. According to equation (61) of [10] the smaller of both R_1 and R_2 has the greater influence on bubble growth, i.e. for $t < t_e$, liquid inertia governs initial bubble growth,

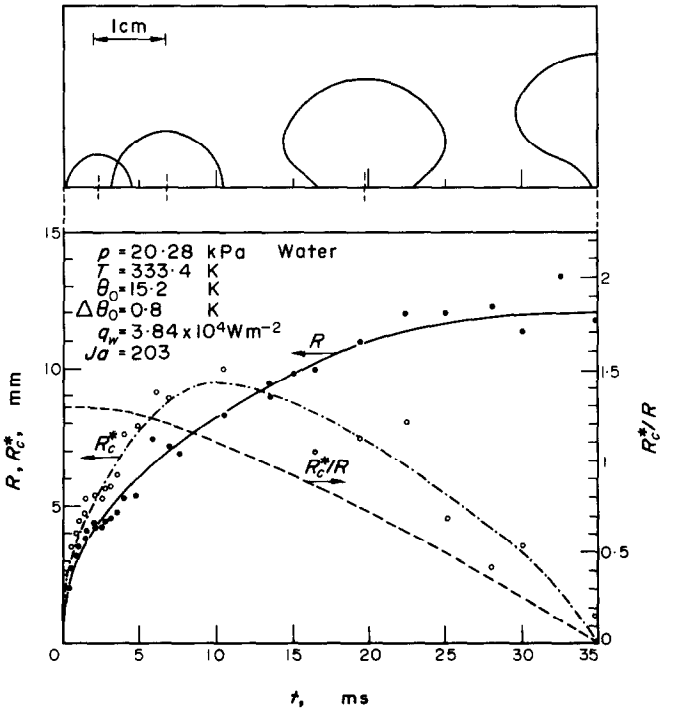

FIG. 4. Water boiling at 20·28 kPa. Equivalent bubble radius, R, contactradius, R_c^*, and ratio, R_c^*/R, in dependence on time. Corresponding bubble profile and limit of mode of hemispherical growth are shown in the upper drawings.

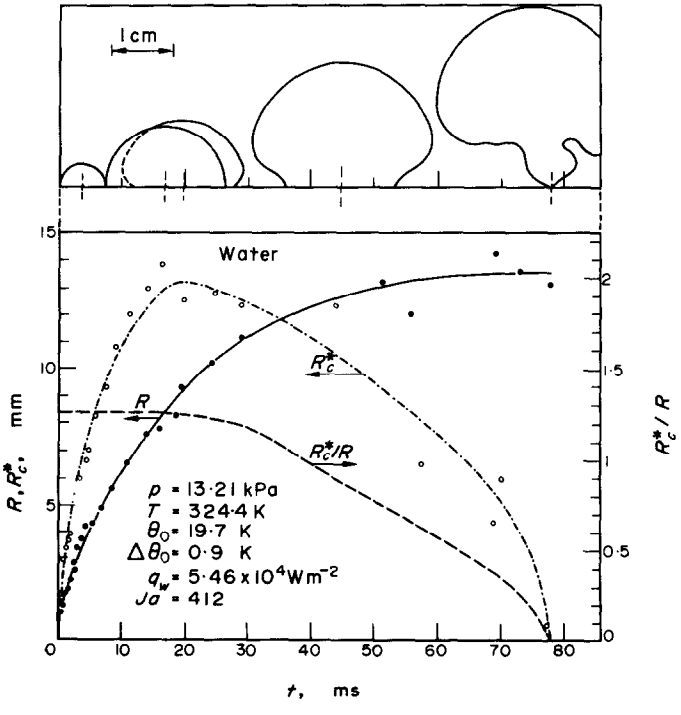

FIG. 5. Water boiling at 13·21 kPa. Equivalent bubble radius, R, contactradius, R_c^*, and ratio, R_c^*/R, in dependence on time. Corresponding bubble profile and limit of mode of hemispherical growth are shown in the upper drawings.

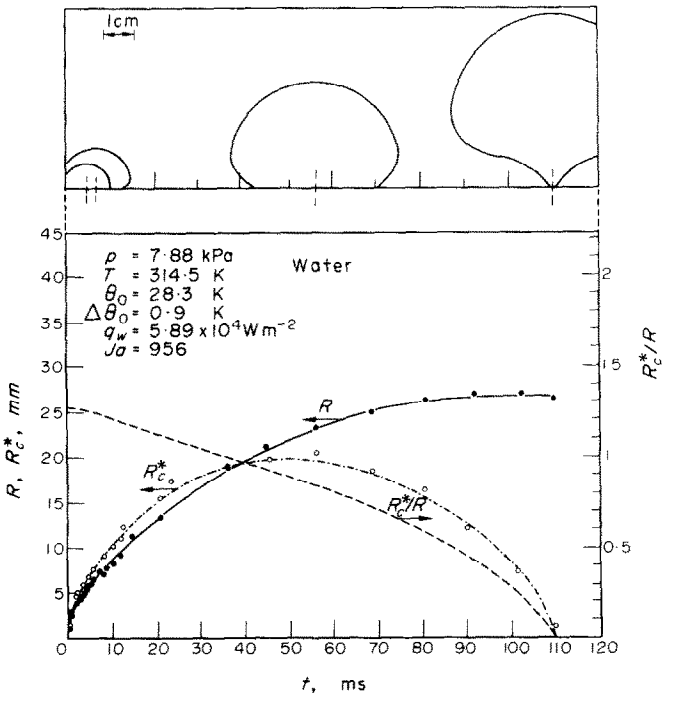

FIG. 6. Water boiling at 7·88 kPa. Equivalent bubble radius, R, contactradius, R_c^*, and ratio, R_c^*/R, in dependence on time. Corresponding bubble profile and limit of mode of hemispherical growth are shown in the upper drawings.

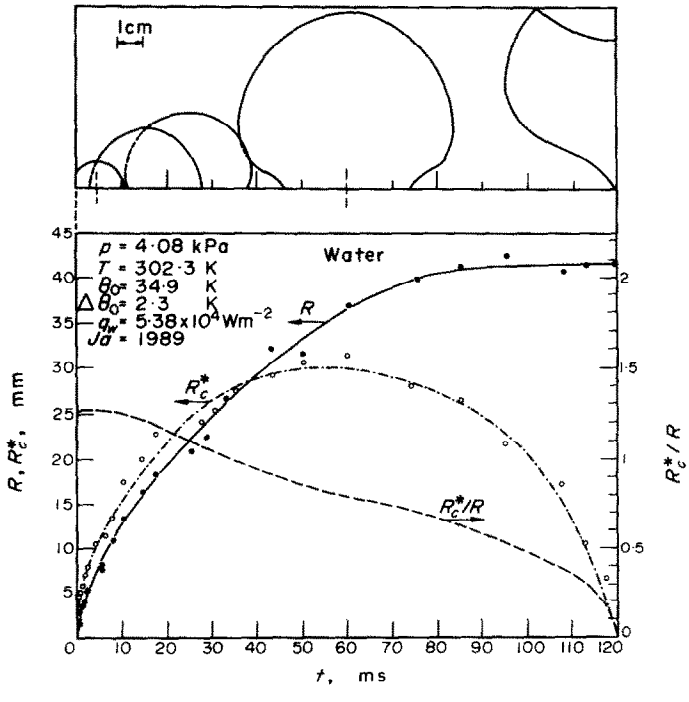

FIG. 7. Water boiling at 4·08 kPa. Equivalent bubble radius, R, contactradius, R_c^*, and ratio, R_c^*/R, in dependence on time. Corresponding bubble profile and limit of mode of hemispherical growth are shown in the upper drawings.

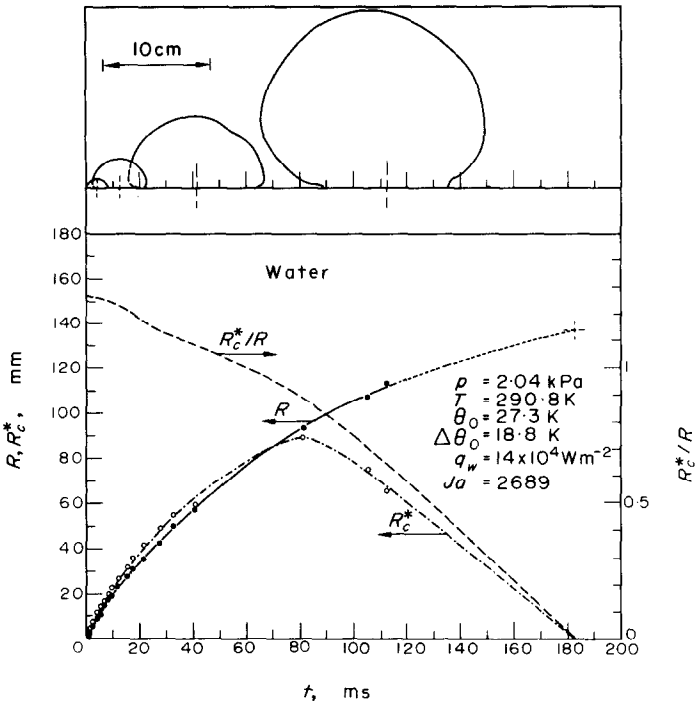

FIG. 8. Water boiling at 2·04 kPa. Equivalent bubble radius, R, contactradius, R_c^*, and ratio, R_c^*/R, in dependence on time. Corresponding bubble profile and limit of mode of hemispherical growth are shown in the upper drawings.

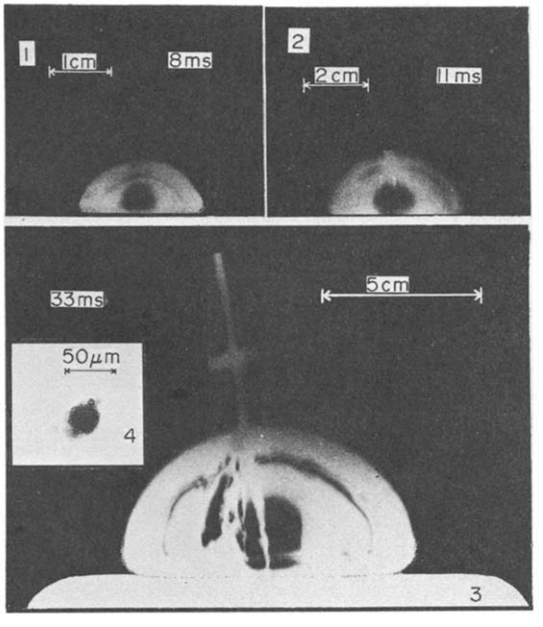

FIG. 9. Water boiling at 26·72 kPa (1) and at 2·04 kPa (2, 3). (1–3): Initial mode of hemispherical growth of adhering vapour bubble; (4): artificial nucleus.

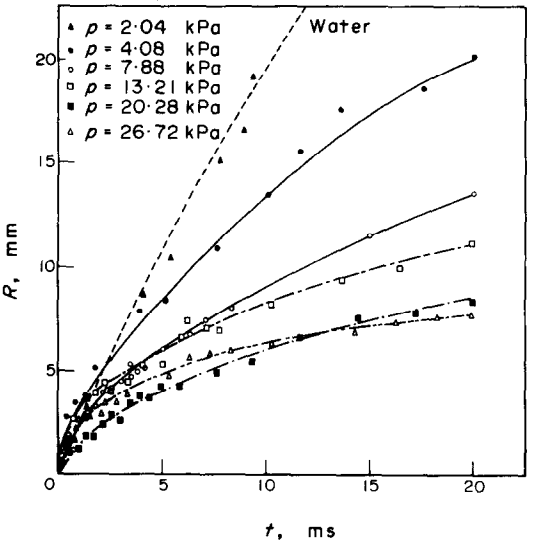

FIG. 10. Water. Initial bubble growth curves for various subatmospheric pressures.

whereas heat diffusion dominates during advanced bubble growth occurring for $t > t_e$.

At pressures below approximately 2·5 kPa, $t_e > t_1$ (Fig. 12 and Table 1), whence the Rayleigh solution governs bubble growth during the entire adherence time, cf. Fig. 8 and the photographs (Figs. 13 and 14) showing "Rayleigh" vapour bubbles in water boiling at 2·04 kPa.

The most striking feature of the growth curves is the following (Figs. 3–8 and 11, 12): both the departure time and the departure radius increase substantially on decreasing pressure. Also, in general, the slope of a

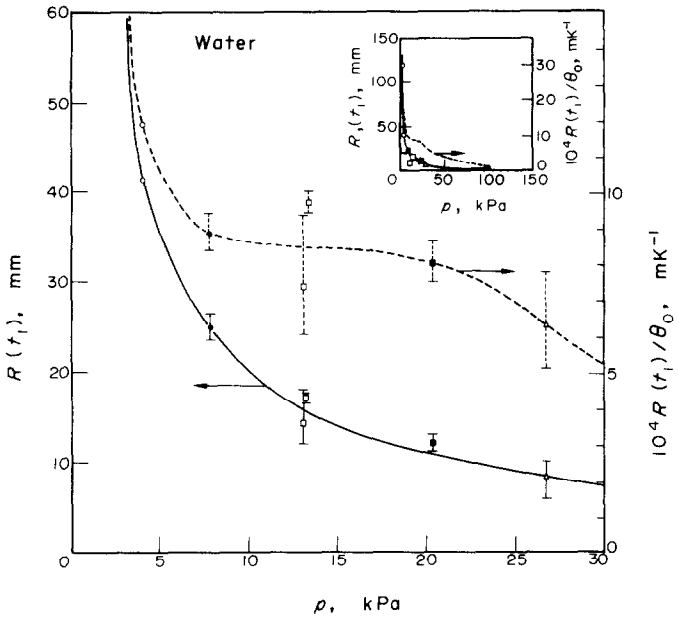

FIG. 11. Water. Equivalent bubble departure radius, $R(t_1)$, and ratio, $R(t_1)/\theta_0$, in dependence on pressure.

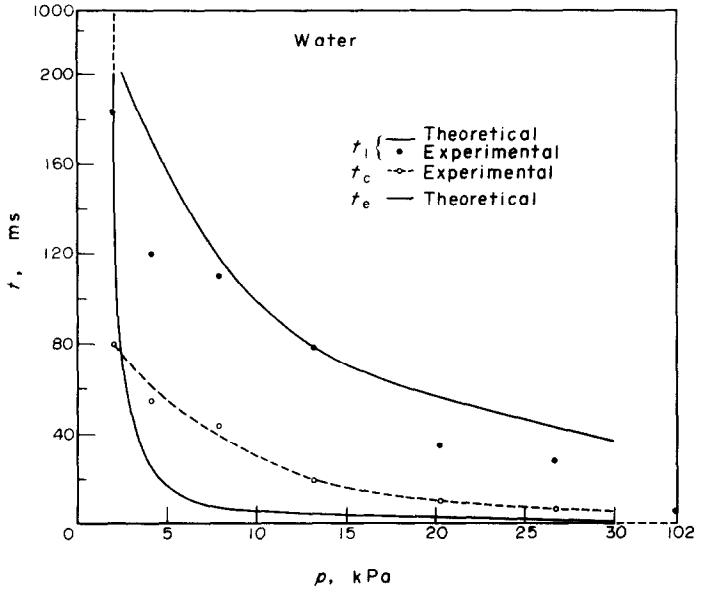

FIG. 12. Water. Bubble departure time, t_1, time of maximum contactradius, t_c, and t_e in dependence on pressure. The theoretical t_1 follows from equation (32) of [10].

growth curve (i.e. the bubble growth rate) at constant pressure decreases gradually with increasing time up to departure (Figs. 3–8, 10). At the pressures represented in Figs. 3–7, the bulk liquid superheating $\Delta\theta_0 \sim 1$K, whence the slope of the growth curves tends to zero at the departure time. Only in case of the lowest pressure investigated (2 kPa, Fig. 8), the bulk liquid was nearly uniformly superheated at the wall superheating, i.e. $\Delta\theta_0 \sim \theta_0$; in this case, bubble growth continues substantially after departure.

3.2 *Radius of contact area*

Figures 3–8 show also the actual radius $R_c^*(t)$ of the contact area between bubble and heating surface. Obviously, during the hemispherical growth period, $R_c^*/R = 2^{1/3} = 1{\cdot}26$. Afterwards, R_c^*/R decreases approximately linearly with exception of the final period shortly before bubble departure, during which a higher contraction rate of the contact area is shown.

A maximum value of the contact radius R_c^* occurs at increasing time t_c (from 7 to 80 ms) at decreasing

Table 1. Water Survey of influential and characteristic parameters for bubble behaviour during nucleate boiling in saturation at subatmospheric pressures. The inserted experimental values of t_1, t_c and $R(t_1)$ are taken from Figs. 3–7. The numbers of the equations refer to van Stralen, Sohal, Cole and Sluyter [10].

Pressure p (kPa)	Bubble growth parameter b eq. (31)	Bubble growth parameter b^* eq. (67)	Maximum height of relaxation microlayer $H_1 = 2b^*R(t_1)$ (mm) eq. (60)	Maximum height of relaxation microlayer $H_1 = 2b^*R(t_1)$ (mm) eq. (38)†	Ratio of evaporation to relaxation microlayer contribution to bubble growth eq. (59)	Bubble departure time t_1 theor. (ms) eq. (32)	Bubble departure time t_1 exper. (ms)	Time t_e of $R_1 = R_2$ theor. (ms)	Time t_e of max. contact area exper. (ms)	Ratio of time of maximum contact area to departure time t_c/t_1 exper.	Ratio of time of maximum contact area to departure time t_c/t_1 theor. eqs. (69), (70)	Thickness of thermal boundary layer $d_{w,co}$ (μm) eq. (32)	Max. initial thickness of evaporation microlayer $d_0\{R_c^*(t_c)\}$ (μm) eqs. (19), (20)	Max. thickness ratio $d_0\{R_c^*(t_c)\}/d_{w,co}$ eq. (68)
26·72	1·758	1·595	25·2	7·8	0·102	35	28	1·75	7	0·25	0·24	183	168	0·92	1·00
20·28	1·335	1·172	27·9	12·4	0·139	72	35	3·0	10	0·29	0·24	273	199	0·73	1·00
13·21	0·501	0·342	9·3	11·9	0·464	79	78	4·9	19	0·24	0·23	273	278	1·02	1·00
7·88	0·354	0·198	10·6	16·6	0·791	100	110	6·9	48	0·44	0·28	303	411	1·36	1·00
4·08	0·304	0·154	12·8	24·1	0·966	178	120	25	55	0·46	0·28	407	418	1·03	1·00
2·04	2·684*	2·547†					183	10^3	80	0·44	0·35	629			

*This value approaches $e = 2{\cdot}718$ due to the large superheating $\Delta\theta_0 = 18{\cdot}8$ K of the bulk (Fig. 8 and Table 2).
†θ_0 has been replaced by the superheating required for formation of the theoretical equilibrium radius, cf. Table 2.

Table 2. Water. Survey of experimental data on vapour bubbles shown in Figs. 3–8

Pressure p (kPa)	Wall superheating θ_0 (K)	Minimum superheating required to activate artificial cavity with mouth radius of 12·5 μm (K) Equation (38) of [10]	Bulk superheating $\Delta\theta_0$ (K)	Bubble departure time t_1 (ms)	Equivalent bubble departure radius $R(t_1)$ (cm)	Bubble departure volume $\frac{4\pi}{3}\{R(t_1)\}^3$ (cm^3)	Bubble enthalpy $\frac{4\pi}{3}\rho_2 l\{R(t_1)\}^3$ (J)
101·3*	21·5	2·6	0·4	6·73	0·092	$3{\cdot}26 \times 10^{-3}$	$4{\cdot}40 \times 10^{-3}$
26·72	12·2	6·8	1·2	28	0·79	2·065	0·954
20·28	15·2	10·1	0·8	35	1·19	7·059	2·103
13·21	19·7	22·2	0·9	78	1·36	10·54	2·083
7·88	28·3	35·5	0·9	110	2·68	80·63	9·893
4·08	34·9	59·2	2·3	120	4·15	299·4	21·82
2·04	27·3†	100·7	18·8	183	15·39	15269	646·9

*cf. [11–13].
†Bubble is generated using hot-wire anemometer in superheated liquid above artificial cavity.

pressure in the investigated range. Apparently, this instant is proportional to the increasing departure time (Fig. 12), cf. equations (69) and (70) of [10]. Comprehensive information on experimental data in comparison to theoretical predictions is given in Tables 1 and 2.

3.3 *Bubble frequency*

In relation to the dependence of the departure time on pressure, the bubble frequency on the artificial nucleation site decreases substantially with decreasing pressure. In the range from 27 to 20 kPa the bubble frequency is of the order of 1–10 Hz; more accurately, it decreases from 5·7 to 2·8 Hz.

At the lowest pressures investigated (2 and 4 kPa), the average waiting time between succeeding bubbles has been extended to exceptional high values of the order of 10–100 s. This curious behaviour is attributed to the relatively slow heat penetration through the copper cylinder, the top face of which is cooled to approximately the corresponding saturation temperature of water during bubble adherence. The penetration depth (i.e. here the distance between the upper side of the cartridge heaters and the cylinder top face) amounts to 0·13 m (Fig. 1), which equals $2(a_w t_2)^{1/2}$; this results in a predicted waiting time of 40 s, in good agreement with the observations at the lowest pressures, cf. Fig. 18.

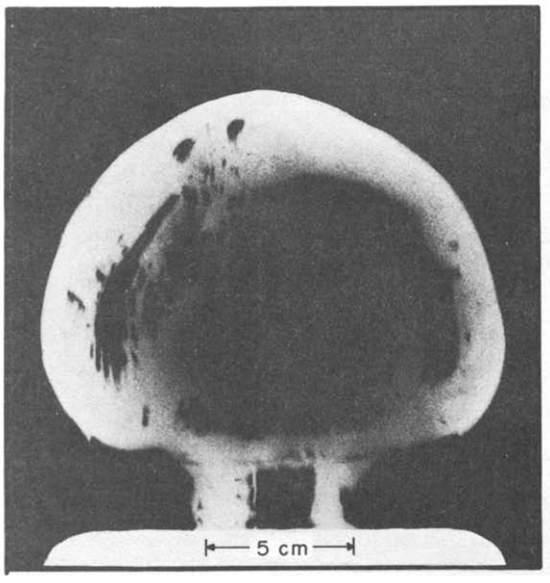

FIG. 13. Water boiling at 2·04 kPa. A large "Rayleigh" vapour bubble shortly before departure. Turbulent eddies are visible.

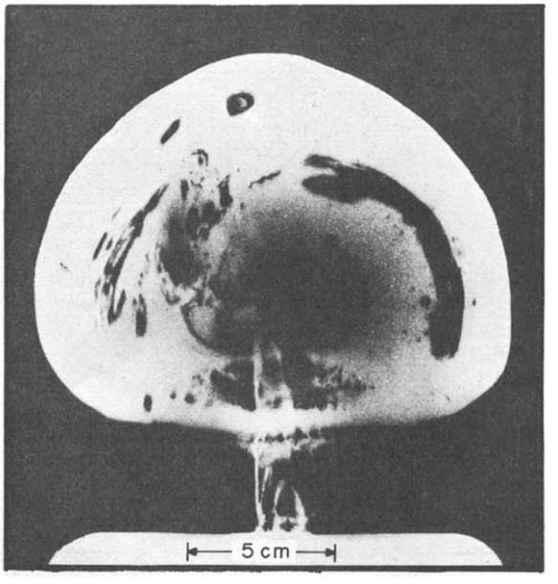

FIG. 14. Water boiling at 2·04 kPa. A thin secondary vapour column succeeds a large "Rayleigh" vapour bubble. Turbulent eddies are visible.

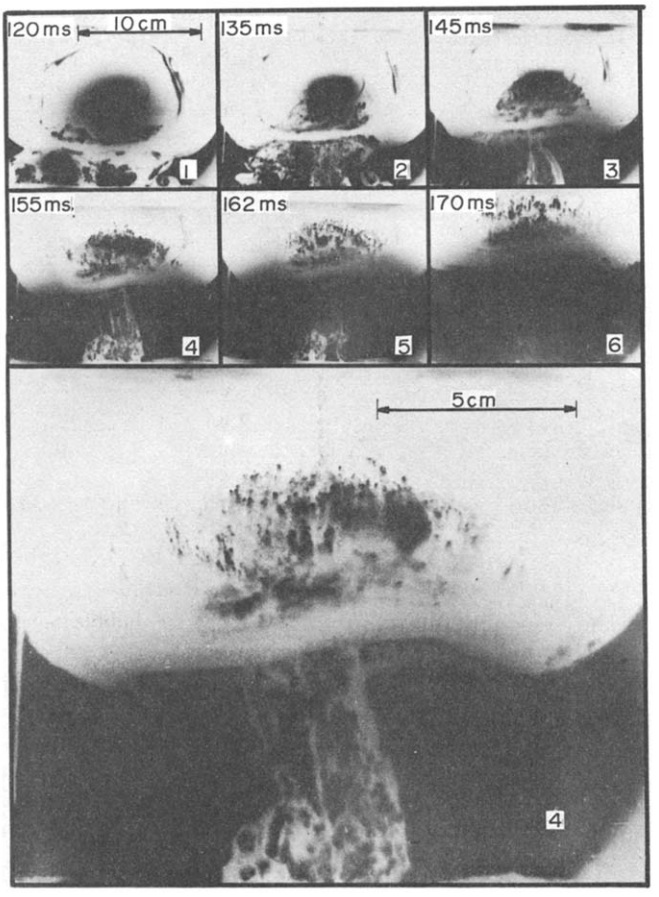

FIG. 15. Water boiling at 4·08 kPa. A high-velocity liquid jet followed by a hot vapour column is penetrating into a large vapour bubble. The lower side of the bubble shows an involution.

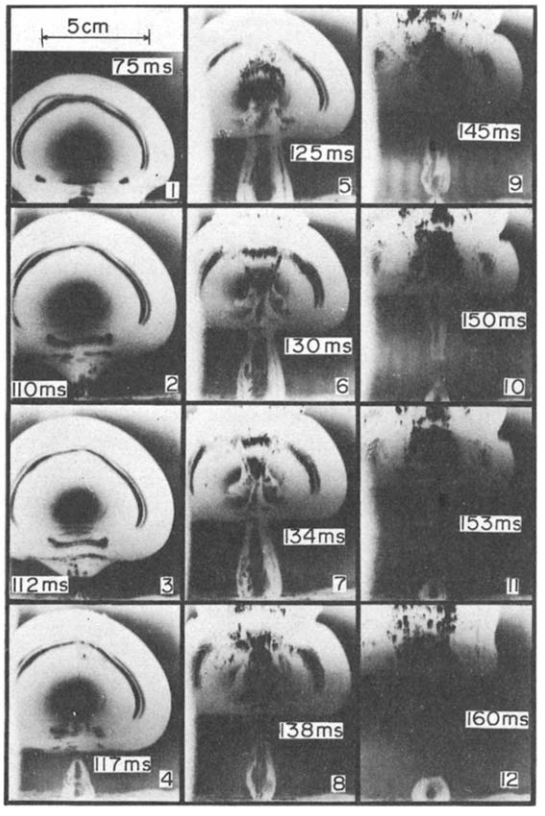

FIG. 16. Water boiling at 7·88 kPa. A diverging high-velocity liquid jet followed by a hot vapour column is penetrating through a large vapour bubble.

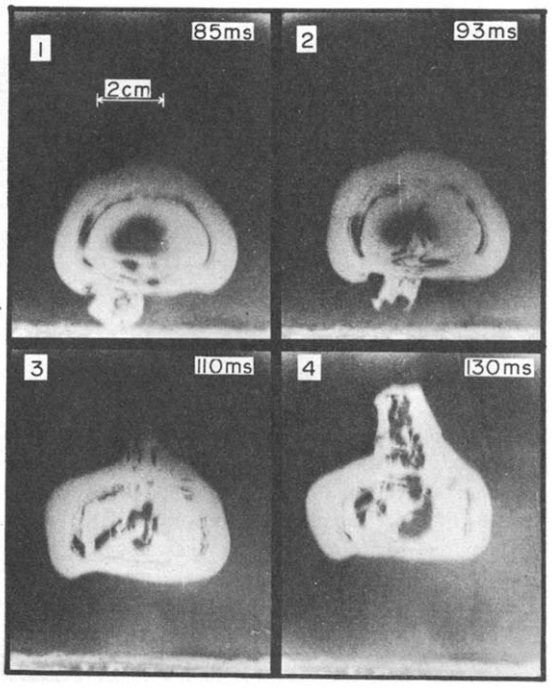

FIG. 17. Water boiling at 13·21 kPa. A high-velocity liquid jet (without secondary vapour column) is penetrating into a relatively large vapour bubble.

3.4 *The curious bubble cycle at 2–8 kPa*

In general, directly after departure of a large bubble, an initially very rapidly growing thin vapour column occurs at the nucleation site (Figs. 13–16). This secondary bubble penetrates into the flattened lower boundary of the preceding large bubble.

Actually, a secondary bubble is not present at the investigated higher pressures of 13–27 kPa (Fig. 17). Obviously, the following two, originally different phenomena interact at the lowest pressures:

(i) In a study of the present high-speed motion pictures, Van Leeuwen [16] observed, that a thin high-velocity liquid jet is formed in the wake of the departed large primary bubble and penetrates into the flat lower side of the bubble, occasionally even penetrating through the upper bubble cap. This behaviour is similar to cavitation, where jet velocities up to 100 m/s have been observed in translating bubbles collapsing due to a pressure step [17, 18]. The high jet velocity corresponds at low ambient pressures to relatively large depressions in the wake.

(ii) The curious behaviour of the secondary vapour column (a "Rayleigh" bubble with an excess pressure, cf. Section 3.1) is attributed to the occurrence of a dry area beneath the centre of the growing primary bubble during adherence to the wall, cf. e.g. [10]. The local wall superheating may be kept there at the original value; this is due to the relatively low value of the thermal conductivity of the vapour, and the behaviour is similar to film boiling.

The local depression in the adjacent liquid increases the superheating at the dry spot substantially, and causes a very rapid growth of the vapour column. Apparently, the diameter of the vapour column is limited to approximately the dimension of the dry area (Fig. 14). Due to its excess pressure, the secondary bubble follows the liquid jet immediately.

The absence of a secondary bubble at higher pressures can be explained by considering the diminishing radius of the dry area—cf. the Appendix to [10]—in combination with a decreasing relative depression in the wake.

Conclusion. The occurrence of the liquid jet seems to be of primary importance (being observed both in boiling at all investigated pressures and in cavitation), the secondary bubble is generated only in combination with a (hot) dry spot at the wall.

Figures 15 and 16 illustrate the curious bubble cycle at low subatmospheric pressures. Figure 17 shows a high-velocity liquid jet (in absence of a secondary vapour column) penetrating through a large bubble. Jet velocities of approximately 5 m/s are estimated from the high-speed motion pictures (Figs. 15–17).

Clark and Merte [19] observed a similar complex bubble cycle and also state, that the second bubble is carried by a high-momentum liquid jet formed by the wake of the first bubble. These workers were able to see the rapid motion of the liquid itself in subcooled boiling by injecting dye in the regions of the boiling

action. These liquid motions in subcooling are similar to those occurring in saturated boiling of binary mixtures adjacent to metal heating wires [11].

Radius of dry area. Equation (24) of [10] predicts [by inserting $R(t_1)$ corresponding to Figs. 13 and 14] a radius of dry area $R_d^*(t_1) = 4{\cdot}4$ mm, a value, which is in quantitative agreement with the width of the observed vapour column in Fig. 14.

Turbulent eddies are observed in the neighbourhood of the curved bubble boundary at the lowest pressures investigated (2–4 kPa, cf. Figs. 13 and 14), where the equivalent Reynolds number may be increasing to values of the order of magnitude of 10^4–10^5, cf. Section 5.6 of [10].

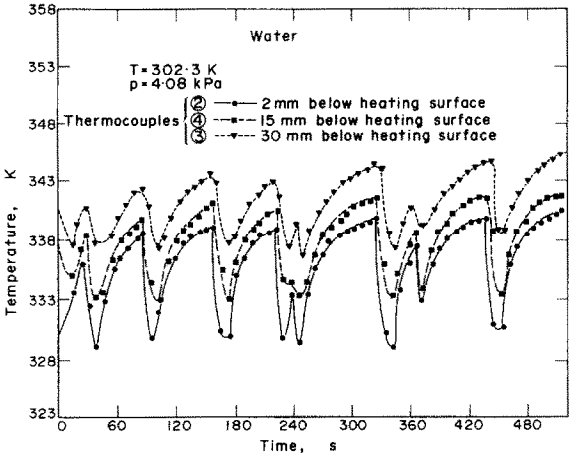

FIG. 18. Water boiling at 4·08 kPa. Temperature fluctuations inside the copper heating cylinder at various distances from the top face.

3.5 *Temperature fluctuations inside the heating cylinder*

At low subatmospheric pressures, substantial temperature fluctuations are observed at the locations of the thermocouples beneath the heating surface (Fig. 18 and Section 5.5 of [10]). Synchronization of these fluctuations to bubble history shows, that the local temperature drops simultaneously during bubble growth and increases again during the succeeding waiting time. These observations are in good agreement with the temperature dips occurring at the heating surface, which have been studied by several investigators, cf. e.g. the literature surveys presented in [10, 11].

The occurrence of the observed periodic temperature fluctuations inside a highly conducting heating material is considered to prove, that the superheating enthalpy of the evaporation microlayer is consumed for the greater part to support bubble growth, cf. Section 5.3 of [10]. Otherwise, in absence of this effect, equation (2) of [10] is predicting a decrease in initial wall superheating θ_0 of only 5 per cent, as for copper in combination with water the ratio of the "contact coefficients" $F_w/F \sim 20$, cf. [11]. Characteristic is the relatively slight damping of amplitude of the fluctuations with the distance from the heating surface. Apparently, this is due to the high thermal diffusivity of copper, which can be seen easily by considering the fluctuations to be harmonic as an approximation, cf. [20]. For the upper thermocouple, which is located 2 mm beneath the artificial nucleation site (Fig. 1), a negligible amplitude damping is calculated (in absence of internal heat sources) at a frequency of 15 mHz (Fig. 18). Actually, periodic fluctuations with amplitudes up to 11 K are observed (Fig. 18) in presence of the bottom cartridge heaters (Section 2.1). Previously, also in the superheated liquid near the heating surface, temperature fluctuations have been observed by van Stralen and Sluyter [14], if the hot junction of a thin thermocouple with short response time is suddenly covered with vapour instead of superheated liquid. These observations formed a direct experimental proof of the physical background underlying both the common bubble growth theories [4–6] and the relaxation microlayer theory [11–13].

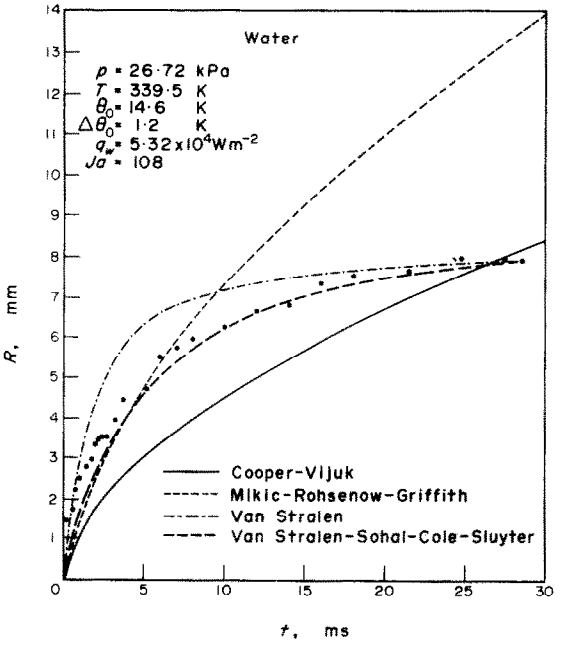

FIG. 19. Water boiling at 26·72 kPa. Experimental bubble growth data up to departure in comparison with theoretical predictions.

4. COMPARISON OF EXPERIMENTAL DATA AND THEORETICAL PREDICTIONS

Stewart and Cole [1] showed the unsuitability of the heat diffusion theories to predict initial hemispherical bubble growth in water during nucleate boiling at 4·9 kPa; in general, theory exceeds experimental data by an order of magnitude, regardless of whether the model is of the uniform superheat [4–6], non-uniform superheat [21] or evaporation microlayer type [22].

Qualitative agreement was observed with models, which combine liquid inertia (the Rayleigh solution R_1) with heat diffusion, the latter being due to the evaporation microlayer [8] or to a relaxation microlayer [7].

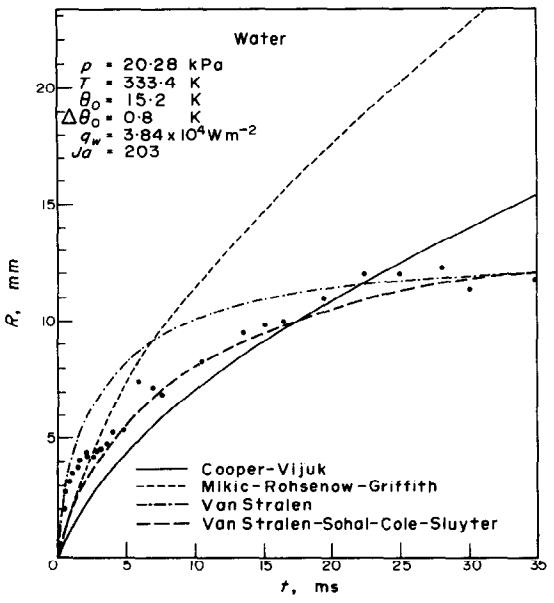

FIG. 20. Water boiling at 20·28 kPa. Experimental bubble growth data up to departure in comparison with theoretical predictions.

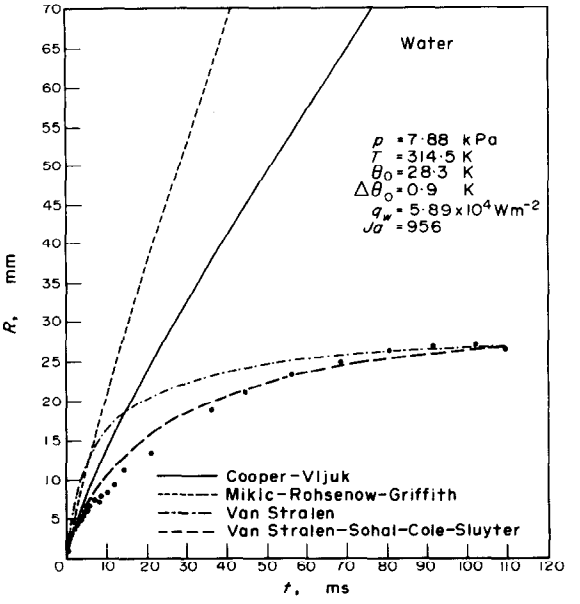

FIG. 22. Water boiling at 7·88 kPa. Experimental bubble growth data up to departure in comparison with theoretical predictions.

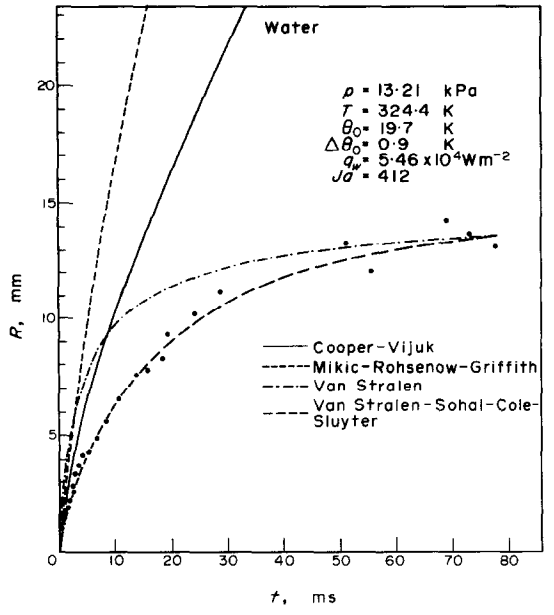

FIG. 21. Water boiling at 13·21 kPa. Experimental bubble growth data up to departure in comparison with theoretical predictions.

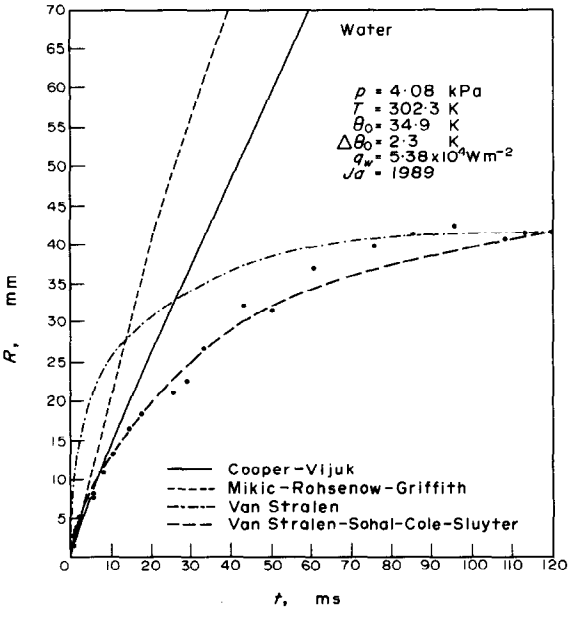

FIG. 23. Water boiling at 4·08 kPa. Experimental bubble growth data up to departure in comparison with theoretical predictions.

In order to compare present experimental data with theory, the numerical values of the appropriate material properties are taken at the average temperature of the thermal boundary layer at the heating wall.

4.1 *The van Stralen relaxation microlayer theory*

Van Stralen's relaxation microlayer model [11–13] is of the diffusion type. Nevertheless, reasonable agreement with experimental data is obtained by fitting the growth parameter b at the instant of bubble departure, cf. Table 1 and Figs. 19–24. Characteristic is the decrease of the numerical value of b with decreasing pressure (Table 1). This is more or less evident by considering the maximum values of H_1 in Table 1 giving an indication of the distance across which the superheated boundary layer can be removed by a growing bubble.

Early bubble growth rates during hemispherical growth ($t < 9$ ms) are overestimated by [11–13] with an average factor of 2.

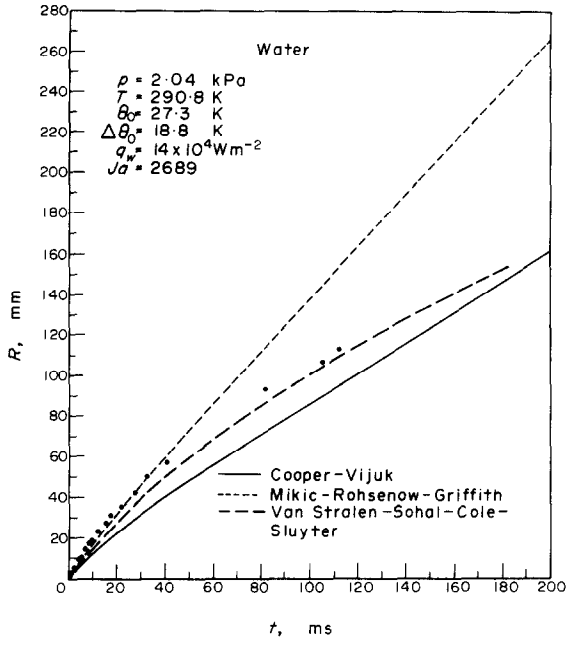

FIG. 24. Water boiling at 2·04 kPa. Experimental bubble growth data up to departure in comparison with theoretical predictions.

4.2 *Models including the effect of liquid inertia*

4.2.1 *The Mikic, Rohsenow and Griffith model* [7]. This theory has been evaluated for infinite waiting time between succeeding bubbles: $t_2 = \infty$, cf. equation (46) of [10]. This restriction is based on the experimental large values of t_2, cf. Section 3.3, but may seem to be in contrast to the small bubble superheatings occurring at pressures of 27–4 kPa, cf. Table 2. However, it has to be realized, that in the present experiments only a thin thermal boundary occurs (Table 1), which is due to convective heat transport. Contrarily, the theory is based on the assumption of a boundary layer being identical with the thermal penetration depth $2(at_2)^{1/2}$. It may be worth noticing here, that equation (46) of [10] simplifies to the Rayleigh solution as $t \to 0$, cf. equation (39) of [10].

At 26·72 and 20·28 kPa (Figs. 19 and 20), predictions agree with the experimental data only during a short initial period of 3 ms. At the instant, t_1, of bubble departure, theory exceeds the experimental value with a factor of 2.

At 13·21 kPa (Fig. 21), the theory overestimates the experimental values during the entire adherence time, at $t = 2$ ms already with a factor of 3. In general, this statement is also true at 7·88 kPa (Fig. 22), the discrepancy being a factor of 4 at $t = 40$ ms.

At 4·08 kPa (Fig. 23), theory agrees with experimental data during the initial 4 ms only, but overestimates afterwards again up to a factor of 4 at $t = 40$ ms. A better agreement is shown at 2·04 kPa (Fig. 24) up to $t = 40$ ms, with an overestimation of a factor of 1·5 at departure.* Apparently, this more satisfactory result is due to the dominating influence of liquid inertia during the entire adherence time, cf. the values of t_e and t_1 in Table 1 and Section 3.1. Moreover, the experimental conditions approximate the uniform superheat case here (Table 2), a circumstance, which improves the reliability of the comparison.

Conclusion. The experimental bubble growth rates are overestimated substantially with the exception of early growth, during which the Rayleigh solution governs. This conclusion is in agreement with previous results of Stewart and Cole [1] obtained at varying values of the waiting time.

4.2.2 *The Cooper and Vijuk model* [8]. Comparison of this combined evaporation microlayer–inertia model has to be limited to the initial mode of hemispherical bubble growth, which occurs during 9 ms, cf. Section 3.1.

At 26·72 kPa, theory underestimates experimental data with a gradually decreasing factor of 2 to 1·5 during an initial hemispherical growth period of 5 ms (Fig. 19). At departure time, quantitative agreement is reached.

Gradually, at decreasing pressure, the theoretical bubble radius increases relatively in comparison to the corresponding experimental value, until finally at 4·08 kPa quantitative agreement is obtained; however, during the initial 10 ms only, i.e. during 8 per cent of the adherence time. The values predicted by the Cooper and Vijuk theory are always below the corresponding values following from the Mikic, Rohsenow and Griffith model.

At 2·04 kPa (Fig. 24) the Cooper and Vijuk theoretical values are slightly below the experimental data. This is, similarly to the case of the Mikic, Rohsenow and Griffith model, obviously due to the substantially dominating influence of liquid inertia, cf. Section 3.4.1 of [10] and equation (61) of [10], which simplifies to the Rayleigh solution—cf. equation (39) of [10]—as $t \to 0$.

4.2.3 *The van Stralen, Sohal, Cole and Sluyter theory* [10]. This recent model is in quantitative agreement with all present experimental data up to departure (Figs. 19–24). It may be worth noticing, that—similar to the parameter b in the van Stralen relaxation microlayer model [11–13]—the numerical values of the time-independent bubble growth parameter b^* (Table 1) are taken from equations (67), (64) and (65) of [10] in order to fit the experimental departure radius $R(t_1)$. This parameter b^* (apparently in relation to b) decreases with decreasing pressure, cf. Table 1 and Section 4.1.

Also, in Table 1, the ratio of the contributions to bubble growth of the evaporation microlayer and the relaxation microlayer is shown. Apparently, this ratio

*The constant in the Rayleigh solution has been taken as the usual value of $(2/3)^{1/2} = 0{\cdot}82$ instead of the proposed value of $(\pi/7)^{1/2} = 0{\cdot}67$, cf. [7], for convenience in comparison with other theoretical models. The conclusions are not violated by this correction.

equals 1 at a pressure of 4 kPa and diminishes to 0·1 at 27 kPa, i.e. this ratio vanishes at atmospheric and higher pressures. The evaporation microlayer is thus of importance only at low subatmospheric pressures. Both the theoretical values of the departure time, t_1, and the ratio, t_c/t_1 (time of maximum contact radius divided by departure time), are in good agreement with experimental results (Table 1 and Fig. 12). Also, the theoretical statement: $d_0\{R^*(t_c)\} = d_{w,co}$ is in fair agreement with the data (Table 1).

4.2.4 *Transition between Rayleigh growth and diffusion-controlled growth.* Both the Cooper and Vijuk [8] and the Van Stralen *et al.* [10] models use the Cooper and Vijuk [8] procedure for the transition bubble growth, cf. equation (26) of [8] and equation (61) of [10].

At present, Zijl [23] is improving the description of this transition, starting from the Navier–Stokes equations, and using a numerical procedure.

Acknowledgements—One of the authors (R. Cole) was privileged to spend a full year (1971–1972) on sabbatical leave at Eindhoven University. M. S. Sohal acknowledges the receipt of a Research Fellowship from Eindhoven University during 1972–1973.

The authors are indebted to several staff members of the C.T.D. ("Centrale Technische Dienst") of Eindhoven University for technical advice and for construction of the boiling apparatus.

The H.T.S. ("Hogere Technische School") students R. P. Brouwer, M. J. M. Schaeken and H. van Doveren assisted in carrying out experiments and performed the frame by frame analysis of the high speed films.

REFERENCES

1. J. K. Stewart and R. Cole, Bubble growth rates during nucleate boiling at high Jakob numbers, *Int. J. Heat Mass Transfer* **15**, 655–663 (1972).
2. R. Cole and H. L. Shulman, Bubble growth rates at high Jakob numbers, *Int. J. Heat Mass Transfer* **9**, 1377–1390 (1966).
3. S. J. D. van Stralen, Comments on the paper "Bubble growth rates at high Jakob numbers", *Int. J. Heat Mass Transfer* **10**, 1908–1912 (1967).
4. H. K. Forster and N. Zuber, Growth of a vapour bubble in superheated liquid, *J. Appl. Phys.* **25**, 474–478 (1954).
5. M. S. Plesset and S. A. Zwick, The growth of vapour bubbles in superheated liquids, *J. Appl. Phys.* **25**, 493–500 (1954).
6. L. E. Scriven, On the dynamics of phase growth, *Chem. Engng Sci.* **10**, 1–13 (1959).
7. B. B. Mikic, W. M. Rohsenow and P. Griffith, On bubble growth rates, *Int. J. Heat Mass Transfer* **13**, 657–666 (1970).
8. M. G. Cooper and R. M. Vijuk, Bubble growth in nucleate pool boiling, in *Proc. 4th Int. Heat Transfer Conf., Paris—Versailles*, Vol. V, B 2.1, pp. 1–11. Elsevier, Amsterdam (1970).
9. Lord Rayleigh, On the pressure developed in a liquid during the collapse of a spherical cavity, *Phil. Mag.* **34**, 94–98 (1917); *Scientific Papers*, Vol. 6. Cambridge University Press, Cambridge (1920).
10. S. J. D. van Stralen, M. S. Sohal, R. Cole and W. M. Sluyter, Bubble growth rates in pure and binary systems: combined effect of relaxation and evaporation microlayers, *Int. J. Heat Mass Transfer* **18**, 453–467 (1975).
11. S. J. D. van Stralen, The mechanism of nucleate boiling in pure liquids and in binary mixtures, Parts I–IV, *Int. J. Heat Mass Transfer* **9**, 995–1020, 1021–1046 (1966); **10**, 1469–1484, 1485–1498 (1967).
12. S. J. D. van Stralen, The boiling paradox in binary liquid mixtures, *Chem. Engng Sci.* **25**, 149–171 (1970).
13. S. J. D. van Stralen, The boiling paradox in binary systems, in *Proc. 4th Int. Heat Transfer Conf., Paris—Versailles*, Vol. VI, B 7.6, pp. 1–12. Elsevier, Amsterdam (1970); *ibid.* Vol. X, pp. 241–249 (1971).
14. S. J. D. van Stralen and W. M. Sluyter, Local temperature fluctuations in saturated pool boiling of pure liquids and binary mixtures, *Int. J. Heat Mass Transfer* **12**, 187–198 (1969).
15. S. J. D. van Stralen, W. M. Sluyter and R. Cole, Bubble growth rates in nucleate boiling of the binary system water–2-butanone at subatmospheric pressures, *Int. J. Heat Mass Transfer* **18** (1975). To be published.
16. H. J. W. van Leeuwen, Transportphysics Section, Eindhoven University of Technology, private communication (1973).
17. P. T. Smulders, Transportphysics Section, Eindhoven University of Technology, Private communication (1973).
18. W. A. H. J. Hermans, On the stability of a translating gas bubble under the influence of a pressure step, Doctor thesis, Eindhoven University of Technology (1973).
19. J. A. Clark and H. Merte, University of Michigan, Ann Arbor, Michigan, Private communication by J. A. Clark (1973).
20. B. Gebhart, *Heat Transfer*. McGraw-Hill, New York (1961).
21. B. B. Mikic and W. M. Rohsenow, Bubble growth rates in non-uniform temperature field, *Progress Heat and Mass Transfer*, Vol. 2, pp. 283–293. Pergamon, Oxford (1969).
22. M. G. Cooper, The microlayer and bubble growth in nucleate pool boiling, *Int. J. Heat Mass Transfer* **12**, 915–933 (1969).
23. W. Zijl, Private communication, Eindhoven University of Technology, Netherlands (1974).